Technical Report:

Precision of the multiway cut using Vector Electrical Flow

Peter J. Yim[a,**]

[a]912 Primrose Ct., Belle Mead 08502, USA

ABSTRACT

Vector Electrical Flow is a proposed multiway cut solution. The goal of this study was to perform robust testing of this algorithm. The algorithm was applied unstructured and a structured graph with random weights and graphs from applications in dense stereo matching and image denoising. The study found that the Vector Electric Flow solution was within 0.65 ± 0.54% of the known minimum-weight multiway cut. Based on this testing, Vector Electrical Flow has very strong potential for applications in computer vision. **September 6, 2020**

1. Introduction

A powerful approach to computer vision inference involves minimization of the generalized Potts Energy:[1]

$$f(\boldsymbol{\ell}) = \sum_{i \in V_0} f_p(\ell_i) + \sum_{\{i,j\} \in E_0} \lambda_{\{i,j\}}[\ell_i \neq \ell_j] \qquad (1)$$

where the function expresses the cost of the assignment of a set of labels $\ell \in L$ to the nodes of a graph $G_0 = (V_0, E_0)$. f_i and $\lambda_{\{i,j\}}$ are positive functions. In the case of computer vision, the function f_i and $\lambda_{\{i,j\}}$ are related to the image intensities. The bracket notation means the following: $[\cdot]$ is 1 if the condition is true and 0 otherwise.

For the case of $|L| = 2$, the Potts energy can be minimized exactly by the graph cut algorithm (12). In the case for $|L| > 2$, the optimal solution can only be obtained for special cases such as where the labels are ordered (14), where the graph is sequential (8), or where the graph has a tree structure(9). An early approach based on linear programming was also developed with theoretical worst-case bounds (15).

Approximation methods have also been developed based on the graph cut; α-expansion (3) and α-β - swap (3), and based on tree reweighted message passing (19) and sequential tree reweighted message passing in particular (16). These methods do also apply to Markov random field models of images that have more general pair-wise energy functions.

More recent focus has been on improvements to the computation speed (24) (6) (25) (1) (10), (17).

Our contribution is to evaluate the accuracy of a novel method for minimization of the Potts energy (22). The method makes use of the equivalence between minimization of the Potts energy and the finding the multiway cut. Importantly, the method is based on the iterative solution of systems of linear equations that makes it potentially amenable to a high-performance computing implementation. The method extends an earlier graph cut algorithm (20) (21).

2. Background

2.1. The Multiway Cut

Our work is based on the observation that minimization of the Potts Energy is equivalent to finding the multiway cut when the graph is modified as described below (4). The multiway cut is applied to a graph $G = (V, E, w)$ derived from G_0. The nodes of the graph obtained by adding nodes corresponding to the set of labels L. These nodes are referred to as terminal nodes, T. Edges are added to the original graph that connect each terminal node to each of the original nodes: $E_T = \{\{t, i\} | t \in T, i \in V_0\}$. The edge weights are defined in a straightforward manner from D_i and $\lambda_{\{}i, j\}$ as described in (4).

**Corresponding author:
e-mail: yimpjp@virtualscalpel.com (Peter J. Yim)

[1]Other forms for the Potts Energy are also in use in computer vision. See (23) and (18).

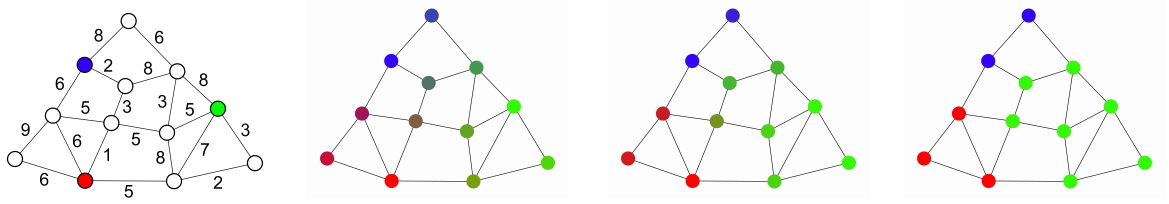

Fig. 1: Application of Vector Electrical Flow to a three terminal planar graph (left). The graph is undirected and has positive edge weights. The voltage state is shown after 1, 5 and 25 iterations starting at figure 2nd to the left. The voltages are three component vectors and are represented by the red, green and blue components of the color at each node. The graph is subdivided into three parts each containing one terminal. The component of the voltage which is maximal at any given node represents the labeling of the node.

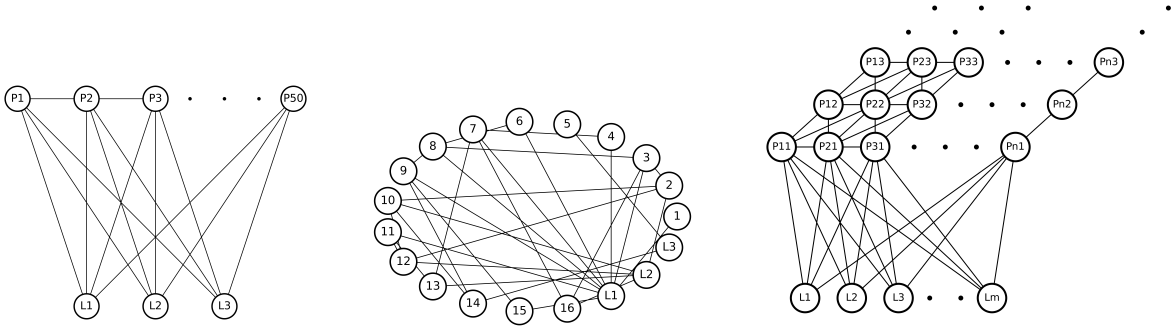

Fig. 2: Graph types used in the evaluation were a sparse unstructured graph (left), a sequence graph with 50 nodes fully interconnected with 3 terminal nodes (center) and an image graph fully interconnected with N terminal nodes (right). In the latter graph interconnections between the image graph nodes and the terminal nodes are only shown for the nodes in the first row of the image graph.

A cut C is defined as a subset of the edges in the graph whose removal from the graph produces a graph consisting of $|T|$ connected components and each connected component contains one node from the set T A minimum-weight graph cut or the multiway cut is a cut that has a minimum weight of all the possible graph cuts:

$$C_{min} = \underset{C \in \Psi}{\operatorname{argmin}} \sum_{\{i,j\} \in C} w_{\{i,i\}} \tag{2}$$

where Ψ is the set of all possible cuts.

The first approximate solution was proposed by Dahlhaus et al (7).

2.2. Cederbaum's Maximum Flow theorem

Cederbaums's Maximum Flow theorem (5) states that the maximum flow in a flow graph can be found by an analog electrical network. The network is defined in the following manner:

- The network is topologically equivalent to the flow graph.
- An external voltage is applied between the terminals that are the s and t nodes in the flow graph.
- A two terminal device connects each node of the network. The current-voltage relationship in the device is monotonically increasing and the current is limited to the weight of the corresponding edge in the flow graph. In the case where the flow graph is undirected, the current is given by the function:

The solution is approximate and the maximum flow solution approaches the exact solution as the external voltage approaches infinity. The Simcut algorithm (20) computes the graph cut using this type of network. In the Simcut, the device current-voltage relation is:

$$y_{ij} = \frac{w_{\{i,j\}}}{1 + |x_i - x_j|}(x_i - x_j) \tag{3}$$

2.3. Vector Electrical Flow

An electrical network will be constructed based on the graph. The electrical network is a network of resistors with each resistor representing one of the edges in the graph with the same connectivity as the corresponding edges in the graph. The electrical behavior of the resistors is non-linear and is given by the relation:

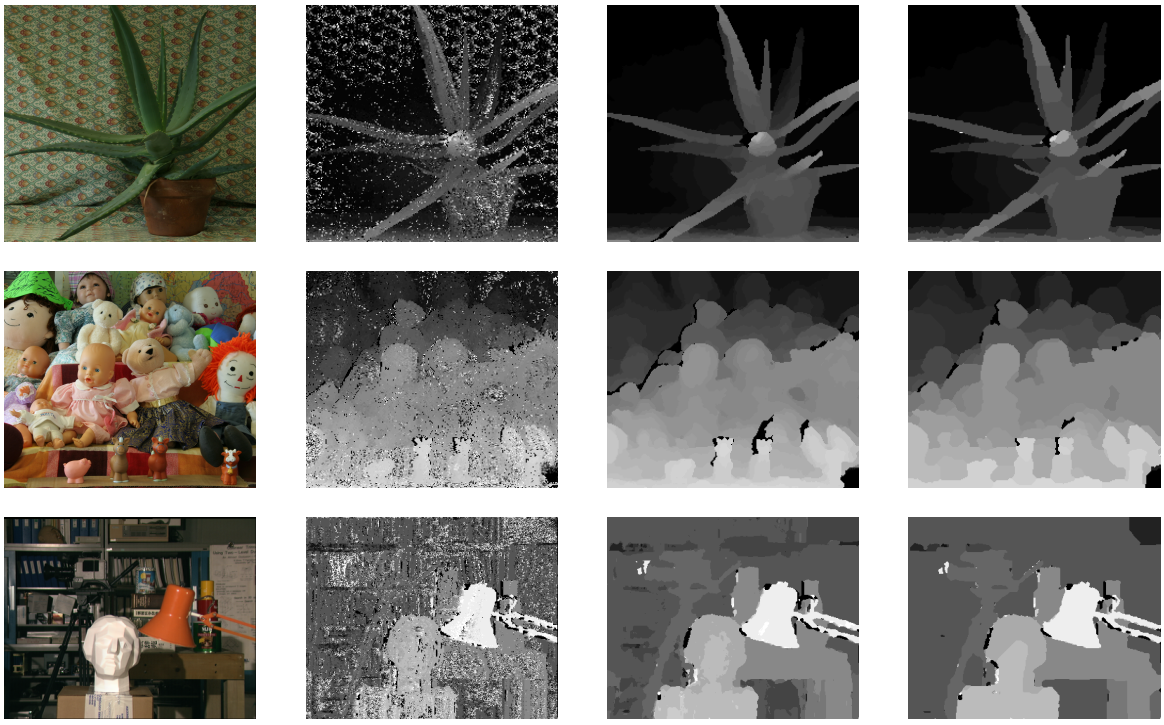

Fig. 3: "Application of vector electrical flow to dense matching. The first column is the original image. THe 2nd through 4th columns are the disparity maps produced by the Multilabel Random Walker algorihm, Vector Electrical Flow and Sequential Tree Reweighted Message Passing, respectively. The datasets were, from the 1st to 3rd row, Aloe, Dolls and Tsukuba, respectively."

$$\mathbf{y}_{ij} = \frac{w_{\{i,j\}}}{1 + \|\mathbf{x}_i - \mathbf{x}_j\|_\infty}(\mathbf{x}_i - \mathbf{x}_j) \tag{4}$$

where $\mathbf{y}$ and $\mathbf{x}$ are vectors with $|L|$ components. The vector $\mathbf{y}$ is analogous to electrical current and the vector $\mathbf{x}$ is analogous to electrical voltage.

The model for the multi-label graph cut is an extension of the binary-valued graph cut model proposed earlier (5).

2.4. The Fixed-Point solution

A matrix is constructed from the graph and is subdivided as follows.

$$\mathbf{A_G}(\mathbf{X}) = \begin{bmatrix} \mathbf{A}_{11} & \mathbf{A}_{12} \\ \mathbf{A}_{21} & \mathbf{A}_{22} \end{bmatrix} \tag{5}$$

The dimension of the blocks $\mathbf{A}_{11}$, $\mathbf{A}_{12}$, $\mathbf{A}_{21}$ and $\mathbf{A}_{22}$ are $N_T \times N_T$, $N_T \times N_0$, $N_0 \times N_T$ and $N_0 \times N_0$ respectively. $N_V = |V|$, $N_0 = |V_0|$ and $N_T = |T|$.

The following notation will be used in referring to graph nodes. An ordering of the graph nodes is defined: $V = \{v_1, v_2 ....v_{N_V}\}$. Also, the first nodes are the terminal nodes: $\{v_i \mid i \leq N_T\} = T$. Based on this ordering, the elements of $\mathbf{A_G}$ are:

$$a_{ij} = \frac{\omega_{\{i,j\}}}{1 + \|\mathbf{x}_i - \mathbf{x}_j\|_\infty} \tag{6}$$

$\mathbf{x}_i$ is the i^{th} row of the matrix $\mathbf{X}$, ω is the edge weight map with respect to the ordered indexing of the graph nodes.

The systems of equations can be written in matrix form:

$$\mathbf{A}(\mathbf{X})\mathbf{X} = \mathbf{B} \tag{7}$$

$\mathbf{A}(\mathbf{X})$ is a $N_V \times N_V$ matrix and $\mathbf{B}$ is a $N_V \times N_T$ matrix.

A system of non-linear equations is derived from the matrix $\mathbf{A}_G$ as follows:

$$\mathbf{A}(\mathbf{X}) = \mathbf{I}_{N_V N_V} \begin{bmatrix} \mathbf{I}_{N_T N_T} & \mathbf{0}_{N_T N_0} \\ \mathbf{A}_{21} & \mathbf{A}_{22} \end{bmatrix} \mathbf{1}_{N_V} - \begin{bmatrix} \mathbf{0}_{N_T N_T} & \mathbf{0}_{N_T N_0} \\ \mathbf{A}_{21} & \mathbf{A}_{22} \end{bmatrix} \tag{8}$$

The constant matrix $\mathbf{B}$ is:

$$\mathbf{B} = v_{in} \times \begin{bmatrix} \mathbf{I}_{N_T N_T} \\ \mathbf{0}_{N_0 N_T} \end{bmatrix} \tag{9}$$

The matrix $\mathbf{B}$ represents an external vector-valued voltage. The first N_T rows of this system of equations have the effect of imposing orthogonal vector-valued voltages at each of the terminal nodes, respectively. The remaining N_0 rows of this system of equations have the effect of imposing flow conservation at each non-terminal node of the electrical network for each component of the electrical flow. A value of 1.0×10^6 was used for v_{in}. For the cases of $N_T = 2$, $v_{in} >> 1$ has the effect of limiting he current through an edge to the weight of the edge.

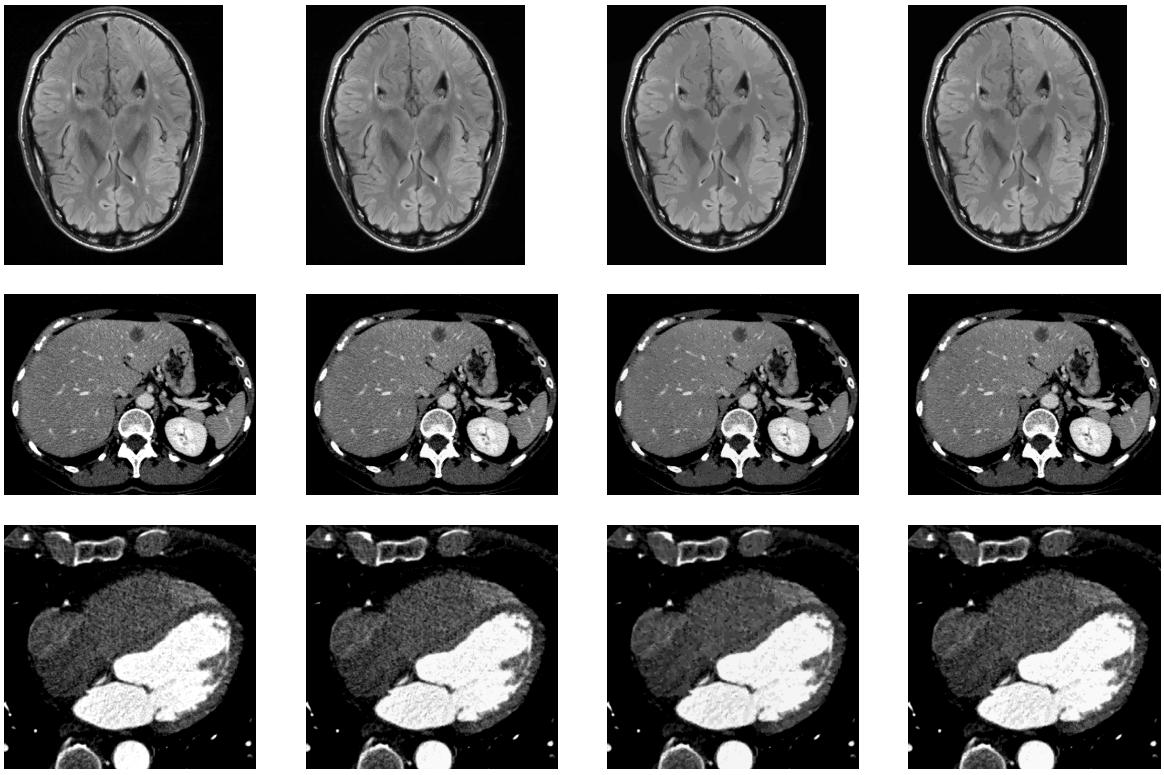

Fig. 4: "Application of Vector Electrical Flow to image denoising. The first column is the original image. THe 2nd through 4th columns are the disparity maps produced by the Multilabel Random Walker algorihm, Vector Electrical Flow and Sequential Tree Reweighted Message Passing, respectively. The datasets were, from the 1st to 3rd row, 1010_brain_mr, 3Dircadb1.1 and Cardix, respectively."

The system of equations is solved using the fixed point method:

$$\mathbf{A}(\widetilde{\mathbf{X}}_k)\widetilde{\mathbf{X}}_{k+1} = \mathbf{B} \tag{10}$$

where $\widetilde{\mathbf{X}}$ is an approximate solution and k is the iteration. The fixed point solution is initialized with the zero matrix $\widetilde{\mathbf{X}}_0 = \mathbf{0}$

Partition of the graph is represented by a vector ℓ :

$$\ell_i^k = \text{argmax}(\widetilde{\mathbf{x}}_i^k)\} \tag{11}$$

where $\widetilde{\mathbf{x}}_p^k$ is the voltage vector at the i^{th} node after the k^{th} iteration and. Note that a single iteration of Vector Electrical Flow is equivalent to the Multi-label Random Walker (13). A stopping criteria of 25 iterations was used in all testing, beyond which negligible change occurred.

3. Benchmarks

3.1. Images

- Aloe. Image data was obtained from the Middlebury Stereo Dataset. These images represent a stereo image pair after epipoloar rectification. The URLs of the left and right image are at the following URL (images view0.png and view1.png respectively).: https:vision.middlebury.edu/stereo/data/scenes2006/FullSize/Aloe/Illum1/Exp1/
- Dolls. The data is from the same source as Aloe. The URLs of the left and right image are at the following URL (images view0.png and view1.png respectively).: https://vision.middlebury.edu/stereo/data/scenes2005/FullSize/Dolls/Illum1/Exp1/
- Tsukuba. The data is from the same source as Aloe. The URLs of the left and right image are at the following URL (images scene1.row3.col1.ppm and scene1.row3.col2.ppm respectively).: https://vision.middlebury.edu/stereo/data/scenes2001/data/tsukuba/
- 1010_braib_mt_04. The image is from a magnetic resonance image of the brain. The 17th 2D section of the 3D image was used. The URL of the dataset is: https://data.idoimaging.com/nifti/1010_brain_mr_04.nii.gz
- 3D-IRCADb-01. The image is from computed tomography of the abdomen. The is the 94th cross-section in the image. The URL is: https://www.ircad.fr/softwares/3Dircadb/3Dircadb1/3Dircadb1.1.zip
- CARDIX. The image from computed tomography of the heart. The 225th cross section of the 3D image was used.

Table 1: Description of graphs using in the Vector Electrical Flow evaluation.

Dataset	Graph type	Nodes	Edges	Terminals / Associations	Neighbor edge weights	Terminal edge weights
Random I	Unstructured	19	32	3 / None	Random Range 0-1	Random Range 0-K
Random II	Signal	53	591	3 / None	Random Range 0-1	Random Range 0-1
Aloe	Stereo matching	52,438	2,618,228	46 / {-49, -48, ... -15 pixels, occlusion}	$C_G = 0.25$ $\sigma = 1000.0$	$C_D = 0.4$ $\sigma = 8.0$
Dolls	Stereo matching	57,322	2,862,362	46 / {-49, -48, ... -15 pixels, occlusion}	$C_G = 0.125$ $\sigma = 1000.0$	$C_D = 0.5$ $\sigma = 8.0$
Tsukuba	Stereo matching	103,408	2,065,901	16 / {-15, -14, ... -1 pixels, occlusion}	$C_G = 0.15$ $\sigma = 1000.0$	$C_D = 0.25$ $\sigma = 10.0$
1010_brain_mr_04	Denoising	55,396	5,749,370	100 / {0, 10, ... 1000 (unitless)}	$C_G = 0.15$ $\sigma = 1000.0$	$C_D = NA$ $\sigma = 10.0$
3Dircadb1.1	Denoising	184370	9,950,690	50 / {0, 5, ... 245 Hounsfield units}	$C_G = 1.0$ $\sigma = 10.0$	$C_D = NA$ $\sigma = 10.0$
Cardix	Denoising	147,506	7,960,322	50 / {0, 10, ... 490 Hounsfield units}	$C_G = 0.25$ $\sigma = 50.0$	$C_D = NA$ $\sigma = 25.0$

The URL is:
http://www.gimias.org/index.php?option=com_content&view=article&id=26&Itemid=18

3.2. Preprocessing of images

The resolution of the left image from the Aloe and Dolls datasets was reduced by a factor of five in both the horizontal and vertical direction. Cropping was applied to the 3D-IRCADb-01 image reducing it from a resolution of 512x512 to 480x384. Cropping was also applied to the Cardix image reducing it from 512x512 to 384x384. The purpose of the reduction in the image resolution and in cropping of the images was to reduce computing memory requirements and computation time. Image intensities in 1010_brain_mr_04, 3D-IRCADb-01 and Cardix were restricted to the ranges [0, 100], [0,245] and [0, 490], respectively. Image intensities above the maximum or below the minimum of the range were reset to the maximum and minimum, respectively, or the range.

3.3. Image to graph mapping

The set of pixels in each image maps in a one-to-one manner onto the nodes of the graph. Pairs of spatially adjacent pixels also map in a one-to-one manner onto the set of edges in the graph. A set of terminal nodes T^{CV} all share edges with all of the nodes corresponding to image pixels V_0^{CV}.

Each edge is assigned a non-negative weight. The edge weights are generally associated with the distance or dissimilarity between the nodes. The distance metric is specific to the type of edge and the graph type. For the distance between neighboring nodes in the graphs arising in noise removal the metric is:

$$\Delta_0^{denoising}(\{p,q\}) = |f(p) - f(q)| \tag{12}$$

Where $f()$ is the image intensity.

For the distance between grid nodes and terminal nodes in graphs from noise removal, the metric is:

$$\Delta_T^{denoising}(\{p,q\}) = |f(p) - \tau(q)| \tag{13}$$

Where τ is the function that associates an image intensity with each element of the set of terminal nodes and $q \in T^{CV}$.

For the distance between neighboring grid nodes in graphs arising from dense stereo matching, the metric is:

$$\Delta_0^{stereo}(\{p,q\}) = \|\boldsymbol{f}(p) - \boldsymbol{f}(q)\|_2 \tag{14}$$

Where $\boldsymbol{f}()$ is the RGB pixel-intensity tuple.

For the distance between grid nodes and the shift-associated terminals in graph, $t \in T^{CV}$ {1} from dense stereo matching the

Table 2: Summary of the evaluation of Vector Electrical Flow. Numbers in parentheses give the precision of final result in comparison to the exact solution, for the Random I and Random II datasets and in comparison to the lower bound of the energy from Sequential Tree Reweighted Message Passing, for the remaining data sets.

Dataset	Exact	Independent pixel model	Multilabel Random Walker	Sequential Tree Re-weighted Message Passing	Vector Electrical Flow
Random I	3.643 ± 0.606	14.697 ± 3.037 (300 %)	5.090 ± 0.816 (39 %)	3.643 ± 0.606 (exact)	3.653 ± 0.618 (0.27 %)
Random II	43.177 ± 3.058	78.886 ± 3.905 (82 %)	48.534 ± 3.602 (12 %)	43.177 ± 3.058 (exact)	43.255 ± 3.074 (0.18 %)
Aloe	NA	538,156 (16 %)	482,528 (4.4 %)	461,932 (0.0025 %)	463,564 (0.35 %)
Dolls	NA	789,495 (12 %)	726,874 (3.4 %)	702,566 (0.0001.5 %)	704,965 (0.34 %)
Tsukuba	NA	868,830 (14 %)	786,451 (3.4 %)	760,015 (0.000053 %)	761,570 (0.20 %)
1010_brain_mr_04	NA	273,304 (45 %)	223,242 (19 %)	187,540 (0.0037 %)	190,044 (1.3 %)
3Dircadb1.1	NA	556,950 (38 %)	460,540 (14 %)	403,711 (0.047 %)	408,029 (1.1 %)
Cardix	NA	503,813 (30 %)	401,775 (4.1 %)	385,675 (0.0015 %)	391,317 (1.4 %)
Mean	NA	(67 ±97%)	(12 ±12%)	(0.0069 ±0.016%)	(0.65 ±0.54%)

distance metric of Birchfield and Tamasi (2) is used but only with interpolation of the right image:

$$\Delta_0^{stereo}(\{p,q\}) = \min_{\delta}(||\boldsymbol{f}(p) - \boldsymbol{g}(p, \tau_{stereo}(q) + \delta)||_2), \quad (15)$$

Where $\boldsymbol{g}$ is the RGB image intensity of the right image, τ_{stereo} is a horizontal shift in pixels and $\delta \in \{-0, 5, 0.0, 0.5\}$ and $q \in T^{CV}$.

The distance function is then related to the edge weight using a Gaussian function:

$$w_{\{p,q\}}^{CV} = c_G e^{-(\frac{\Delta_{\{p,q\}}}{\sigma})^2} \quad (16)$$

Where c_G and σ are constants and Δ represents the distance between the nodes $\Delta_0^{denoising}$, $\Delta_T^{denoising}$, Δ_0^{stereo} or Δ_T^{stereo}. The constants are selected based on trial and error. For the applications to dense stereo matching, one terminal, $t = 1$ is defined to represent "occlusion". $C_G = 1$ for all terminal edge weights. All edges incident to that terminal have a weight of C_D.

3.4. Labeling of Sequences

Vector Electrical Flow was evaluated for labeling of points in a graph composed of a sequence of points and a set of labels. The nodes of the graph are points from the sequence: $V_0^S = \{s_1, s_2, s_3, ...s_N\}$ and from a set of labels T^S. Edges are incident to all of the nodes V_0^S from all of the terminals: $E_T^S = \{\{s_i, q\} \mid (i,q) \in \{1,2,...N\} \times T^S\}$. Edges also are incident to successive elements of the sequence: $E_0^S = \{\{s_i, s_{i+1}\} \mid i \in \{1,2,...N-1\}\}$

The minimum weight graph cut was obtained *via* dynamic programming (11). All edge weights were randomly generated. Evaluation was done on the basis of 10 graphs.

3.5. Labeling of Unstructured Graphs

Vector Electrical Flow was evaluated for labeling of nodes on unstructured graphs. Each graph contained 16 non-terminal nodes V_0^U and 3 terminal nodes, T^U.

20 edges were based on random pairing of the generic nodes, E_0^U. Another 16 edges randomly paired each generic node to one and only one label node or terminal, E_T^U The weight of the edges was:

$$w_{\{p,q\}}^U = \begin{cases} R, \text{ if } \{i,j\} \in E_0^U \\ kR, \text{ if } \{i,j\} \in E_T^U \end{cases} \quad (17)$$

where R is a random variable and k is a factor that balances the weights of the edges E_0^U and E_T^U:

$$\sum_{\{p,q\} \in E_0^U} w_{\{p,q\}}^U = \sum_{\{p,q\} \in E_T^U} w_{\{p,q\}}^U \quad (18)$$

Evaluation was based on the results from labeling of 10 graphs. The exact solution to the multilabel graph cut was determined by exhaustive search.

4. Results

In total, Vector Electrical Flow was evaluated on eight graphs; two generated with random weights, three with dense stereo matching application and three with image denoising application. Descriptions of the graphs are given in table 1.

Results for graphs with random weights are based on the mean results over ten trials. Energy minimization with Vector Electrical Flow was compared with those from an independent-pixel model, with Multilabel Random Walker and the Sequential Tree-Reweighted Message Passing. The independent-pixel

model refers to a model in which all pairwise potentials in the Potts energy are zero. TRW-S was obtained for 250 iterations for all graphs. For the random-weight graphs, exact solutions were obtained by exhaustive search, for the unstructured graph, and by dynamic programming for the graph based on a sequence. Energies are shown in table 2.

Energy minimization by Vector Electrical Flow was superior by a large margin to energy minimization by the independent-pixel model and by Multilabel Random Walker. Energy minimization by Sequential Tree Reweighted Message Passing was nearly exact and was superior to that of Vector Electrical Flow. However, energy minimization by Vector Electrical Flow was very close to optimal with the result differing by $0.65 \pm 0.54\%$. For the graphs from the computer vision applications, the labeling results are shown in figures 3 and 4.

Computations were not optimized for speed but for reference, Vector Electrical Flow required 196 seconds for 25 iterations while TRW-S required 0.6 seconds to obtain comparable precision. That precision was obtained after a single iteration. Timing was based on the Aloe dataset. Processing for both algorithms was on an Amazon EC2 t2.xlarge instance with a 3.3 GHz CPU clock speed.

5. Conclusions

This study establishes that Vector Electrical Flow has exceptional potential for multiway cuts. The practical value of the algorithm, however, is not yet established. One consideration will be whether a fast implementation of the algorithm can be obtained.

Computation of Vector Electric Flow was found to converge in all cases. Intuitively, solution of the systems of equations used in Vector Electric Flow require a conductive path from each node to at least one terminal. That was found to be the case for all testing. Limitation of the range of image intensities in data sets from the image denoising application was necessary to meet this condition. Further mathematical characterization of this algorithm is desirable but is beyond the scope of this study.

References

[1] S. Alchatzidis, A. Sotiras, and N. Paragios. Efficient parallel message computation for map inference. In *2011 International Conference on Computer Vision*, pages 1379–1386, 2011. 1

[2] S. Birchfield and C. Tomasi. Depth discontinuities by pixel-to-pixel stereo. In *Sixth International Conference on Computer Vision (IEEE Cat. No.98CH36271)*, pages 1073–1080, 1998. 6

[3] Y. Boykov, O. Veksler, and R. Zabih. Fast approximate energy minimization via graph cuts. In *Proceedings of the Seventh IEEE International Conference on Computer Vision*, volume 1, pages 377–384, 1999. 1

[4] Y. Boykov, O. Veksler, and R. Zabih. Fast approximate energy minimization via graph cuts. *IEEE Transactions on Pattern Analysis and Machine Intelligence*, 23(11):1222–1239, 2001. 1

[5] I. Cederbaum. On the optimal operation of communication nets. *Journal of the Franklin Institute*, 274:138–141, 1962. 2, 3

[6] J. Choi and R. A. Rutenbar. Fpga acceleration of markov random field trw-s inference for stereo matching. In *2013 Eleventh ACM/IEEE International Conference on Formal Methods and Models for Codesign (MEMOCODE 2013)*, pages 139–142, 2013. 1

[7] E. Dahlhaus, D. S. Johnson, C. H. Papadimitriou, P. D. Seymour, and M. Yannakakis. The complexity of multiterminal cuts. *SIAM J. Comput.*, 23:864–894, 1994. 2

[8] T. J. Darrell, D. Demirdjian, N. Checka, and P. F. Felzenszwalb. Plan-view trajectory estimation with dense stereo background models. *International Conference on Computer Vision*, 2:628–635, 2001. 1

[9] P. F. Felzenszwalb and D. P. Huttenlocher. Pictorial structures for object recognition. *International Journal of Computer Vision*, 61:55–79, 2005. 1

[10] P. F. Felzenszwalb and D. P. Huttenlocher. Efficient belief propagation for early vision. *International Journal of Computer Vision volume*, 70(8,929,636):41–54, 2006. 1

[11] P. F. Felzenszwalb and R. Zabih. Dynamic programming and graph algorithms in computer vision. *IEEE Trans Pattern Anal Mach Intell.*, 33(4):721–740, 2011. 6

[12] L. R. Ford and D. R. Fulkerson. Maximal flow through a network. *Canadian Journal of Mathematics*, 8:399–404, 1956. 1

[13] L. Grady. Multilabel random walker image segmentation using prior models. In *2005 IEEE Computer Society Conference on Computer Vision and Pattern Recognition (CVPR'05)*, volume 1, pages 763–770 vol. 1, 2005. 4

[14] H. Ishikawa. Exact optimization for markov random fields with convex priors. *IEEE Transactions on Pattern Analysis and Machine Intelligence*, 25:1333–1336, 2003. 1

[15] J. Kleinberg and E. Tardos. Approximation algorithms for classification problems with pairwise relationships: metric labeling and markov random fields. *Journal of the ACM*, 49:616–639, 2002. 1

[16] V. Kolmogorov. Convergent tree-reweighted message passing for energy minimization. *IEEE Transactions on Pattern Analysis and Machine Intelligence*, 28(10):1568–1583, 2006. 1

[17] V. Lempitsky, C. Rother, and A. Blake. Logcut - efficient graph cut optimization for markov random fields. In *2007 IEEE 11th International Conference on Computer Vision*, pages 1–8, 2007. 1

[18] C. Nieuwenhuis, E. Töppe, and D. Cremers. A survey and comparison of discrete and continuous multi-label optimization approaches for the potts model. *International journal of computer vision*, 104(3):223–240, 2013. 1

[19] W. J. Wainwright, T. S., Jaakkola, and A. S. Willsky. Tree-based reparameterization framework for analysis of sum-product and related algorithms. *IEEE Trans. Information Theory*, 45:1120–1146, 2003. 1

[20] P. J. Yim. Method and system for image segmentation. *United States Patent*, (8,929,636), 2015. 1, 2

[21] P. J. Yim. Acceleration of the Graph Cut with High Performance Computing. Technical report, Virtual Scalpel, Inc., 11 2016. 1

[22] P. J. Yim. Method and system for multi-label image segmentation. *United States Patent*, (10354391), 2018. 1

[23] J. Yuan, E. Bae, and X. Tai. A study on continuous max-flow and min-cut approaches. In *2010 IEEE Computer Society Conference on Computer Vision and Pattern Recognition*, pages 2217–2224, 2010. 1

[24] W. Zhao, H. Fu, and G. Yang. A fully-pipelined fpga design for tree-reweighted message passing algorithm. In *2014 IEEE 22nd Annual International Symposium on Field-Programmable Custom Computing Machines (FCCM)*, pages 177–177, Los Alamitos, CA, USA, may 2014. IEEE Computer Society. 1

[25] W. Zhao, H. Fu, G. Yang, and W. Luk. Patra: Parallel tree-reweighted message passing architecture. In *2014 24th International Conference on Field Programmable Logic and Applications (FPL)*, pages 1–6, 2014. 1